Conditional Dynamics of Interacting Quantum Dots
Lucio Robledo, *et al.*
Science **320**, 772 (2008);
DOI: 10.1126/science.1155374

Table 1. Nonlinear parameters and phase modulation derived from experimental data for the strongly (first row) and weakly (second row) coupled QDs. $\Delta\phi$ is a maximum differential phase shift [$\Delta\phi = \phi(n_c) - \phi(0)$], which is achieved at the intracavity photon number n_c in the last column.

$g/2\pi$ (GHz)	$\lambda_s - \lambda_{QD}$ (nm)	$\lambda_s - \lambda_c$ (nm)	n_2 (cm^2/W)	$\chi^{(3)}$ (m^2/V^2)	$\Delta\phi$	n_c
16	0.014 (0.3g)	0	2.7×10^{-5}	2.4×10^{-10}	0.015π	0.01
8	0.009 (0.4g)	0.027	1.8×10^{-5}	1.6×10^{-10}	0.05π	0.05

requires coupling efficiencies that are higher than the observed 2 to 5%. This technical challenge can be overcome. We have already demonstrated architecture for a QD cavity-waveguide–coupled quantum network (*24*) with coupling efficiency above 50% between two nodes, and cavity-waveguide couplers (*25*) with coupling efficiency reaching 90%. The observed fluorescence losses are already sufficiently low to allow scalable computation (*26*), and can be further improved with increases in cavity Q. The ability to tailor photon-QD interactions by PC fabrication makes this a highly versatile platform for a variety of quantum optics experiments and has great potential for compact scalable quantum devices.

References and Notes

1. E. Knill, R. Laflamme, G. J. Milburn, *Nature* **409**, 46 (2001).
2. Q. Turchette, C. Hood, W. Lange, H. Mabuchi, H. J. Kimble, *Phys. Rev. Lett.* **75**, 4710 (1995).
3. T. Wilk, S. C. Webster, A. Kuhn, G. Rempe, *Science* **317**, 488 (2007).
4. J. Majer *et al.*, *Nature* **449**, 443 (2007).
5. C. Santori *et al.*, *Phys. Rev. Lett.* **97**, 247401 (2006).
6. M. V. Gurudev Dutt *et al.*, *Science* **316**, 1312 (2007).
7. D. P. DiVincenzo, *Fortschr. Phys.* **48**, 771 (2000).
8. N. Imoto, H. Haus, Y. Yamamoto, *Phys. Rev. A* **32**, 2287 (1985).
9. J. P. Poizat, P. Grangier, *Phys. Rev. Lett.* **70**, 271 (1993).
10. G. Nogues *et al.*, *Nature* **400**, 239 (1999).
11. Y. Akahane, T. Asano, B.-S. Song, S. Noda, *Nature* **425**, 944 (2003).
12. D. Englund *et al.*, *Nature* **450**, 857 (2007).
13. H. Altug, J. Vučković, *Opt. Lett.* **30**, 982 (2005).
14. E. Waks, J. Vučković, *Phys. Rev. Lett.* **96**, 153601 (2006).
15. I. L. Chuang, Y. Yamamoto, *Phys. Rev. A* **52**, 3489 (1995).
16. K. N. W. J. Munro, T. Spiller, *N. J. Phys.* **7**, 137 (2005).
17. R. Boyd, *Nonlinear Optics* (Academic Press, New York, ed. 2, 2003).
18. D. Englund *et al.*, *Phys. Rev. Lett.* **95**, 013904 (2005).
19. E. Waks, J. Vučković, *Phys. Rev. A* **73**, 041803 (2006).
20. S. M. Tan, www.qo.phy.auckland.ac.nz/qotoolbox.html.
21. S. Harris, J. Field, A. Imamoglu, *Phys. Rev. Lett.* **64**, 1107 (1990).
22. K.-J. Boller, A. Imamolu, S. E. Harris, *Phys. Rev. Lett.* **66**, 2593 (1991).
23. M. A. Nielsen, I. L. Chuang, *Quantum Computation and Quantum Information* (Cambridge Univ. Press, Cambridge, UK, 2000).
24. D. Englund, A. Faraon, B. Zhang, Y. Yamamoto, J. Vučković, *Opt. Express* **15**, 5550 (2007).
25. A. Faraon, E. Waks, D. Englund, I. Fushman, J. Vučković, *Appl. Phys. Lett.* **90**, 073102 (2007).
26. E. Knill, *Nature* **434**, 39 (2005).

27. Financial support was provided by the Multidisciplinary University Research Incentive Center for photonic quantum information systems (Army Research Office/ Intelligence Advanced Research Projects Agency Program DAAD19-03-1-0199), Office of Naval Research Young Investigator Award, and NSF grant CCF-0507295. D.E. and I.F. were also supported by a National Defense Science and Engineering Graduate fellowship. Part of the work was performed at the Stanford Nanofabrication Facility of the National Nanotechnology Infrastructure Network supported by the NSF under grant ECS-9731293.

Supporting Online Material

www.sciencemag.org/cgi/content/full/320/5877/769/DC1
SOM Text
Figs. S1 and S2
References and Notes

26 December 2007; accepted 1 April 2008
10.1126/science.1154643

Conditional Dynamics of Interacting Quantum Dots

Lucio Robledo,[1] Jeroen Elzerman,[1] Gregor Jundt,[1] Mete Atatüre,[2] Alexander Högele,[1] Stefan Fält,[1] Atac Imamoglu[1]*

Conditional quantum dynamics, where the quantum state of one system controls the outcome of measurements on another quantum system, is at the heart of quantum information processing. We demonstrate conditional dynamics for two coupled quantum dots, whereby the probability that one quantum dot makes a transition to an optically excited state is controlled by the presence or absence of an optical excitation in the neighboring dot. Interaction between the dots is mediated by the tunnel coupling between optically excited states and can be optically gated by applying a laser field of the right frequency. Our results represent substantial progress toward realization of an optically effected controlled–phase gate between two solid-state qubits.

Self-assembled semiconductor quantum dots (QDs) (*1*) can be manipulated and probed optically, enabling ultrafast coherent control (*2*) and rendering them model systems for solid-state quantum optics (*3*). Particularly promising are quantum dots deterministically charged with a single electron, because the electron spin state is robust against relaxation and decoherence (*4*). In such systems, single-electron spin states can be optically prepared (*5*) and read out (*6*, *7*), allowing demonstrations of optically detected electron spin resonance (*8*) and coherent spin dynamics (*9*). These results established QD spins as promising candidates for solid-state qubits and motivated our research aimed at demonstrating conditional interactions, which is required for implementing two-qubit quantum gates.

In electrically defined QDs, the exchange interaction (*10*) has been used to demonstrate such controlled conditional coupling between electron spins (*11*). However, this mechanism requires fast electrical control over the exchange splitting, which is not feasible in self-assembled QDs (*12*–*14*). An alternative mechanism that has been proposed for coherent coupling of self-assembled QDs (*15*) is based on dipole-dipole interaction (*16*), which can be switched on in sub-picosecond time scales by optically exciting both QDs (*17*). However, for standard vertically coupled QDs, the bare dipole-dipole interaction is typically too weak (smaller than the linewidth of a QD transition) to allow for the accumulation of large conditional phase shifts.

We present an experimental realization of a strong optically gated interaction between a neutral and a single-electron-charged QD. The interaction mechanism, which relies on the tunnel coupling between the dots (*12*–*14*), is tunable and can be much larger than the dipole-dipole interaction. The experiments were performed in a GaAs device (grown by molecular beam epitaxy), containing two layers of self-assembled InGaAs QDs with a nominal separation of 15 nm. QDs in the top layer tend to grow directly on top of QDs in the bottom layer because of the strain field produced by the latter (*14*), resulting in stacks of vertically coupled QDs (CQDs). These QD stacks are embedded in a field-effect structure consisting of an n^+-doped GaAs layer acting as an electron reservoir (with a 25-nm tunnel barrier to the bottom QD layer) and a 4-nm-thick semi-transparent Ti top gate (Fig. 1A). By varying the gate voltage, we can deterministically charge the two dots and tune their relative energy. In order to reach a regime where the electronic energy levels of a stack can be brought into resonance, the size of the bottom QDs has been reduced during growth, leading to an increase of their recombination energy. In the following, we refer to the QDs of a stack as the blue QD (bottom) and the red QD (top). The relatively thick tunnel barrier between the dots [compared with the CQDs used in (*12*, *13*)] assures that

[1]Institute of Quantum Electronics, Eidgenössische Technische Hochschule (ETH)–Zürich, CH-8093 Zürich, Switzerland. [2]Cavendish Laboratory, University of Cambridge, J. J. Thomson Avenue, Cambridge CB3 0HE, UK.

*To whom correspondence should be addressed. E-mail: imamoglu@phys.ethz.ch

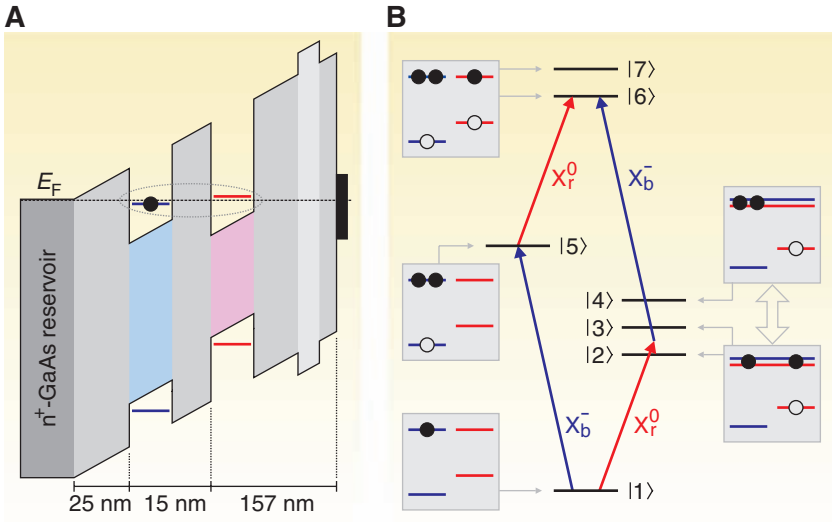

Fig. 1. Conditional interaction in a CQD. (**A**) Schematic band structure of the device, showing the lowest energy levels for electrons and holes confined in the top (red) and bottom (blue) QD. The voltage applied between the gate (black) and the n^+-GaAs reservoir tilts the bands and thereby controls the charge state of the dots and their detuning, allowing the electronic energy levels to be brought into resonance. (**B**) Schematic energy level diagram representing the relevant elementary optical excitations in both dots. The ground state consists of a single electron in the blue dot. X_r^0 corresponds to the creation or recombination of one electron-hole pair in the otherwise empty red dot; X_b^-, to the creation or recombination of an electron-hole pair in the blue dot in the presence of a resident electron. Note that X_r^0 is split because of the bare electron-hole exchange interaction (levels |6⟩ and |7⟩) or because of the exchange interaction plus additional mixing with the interdot exciton (levels |2⟩, |3⟩, and |4⟩).

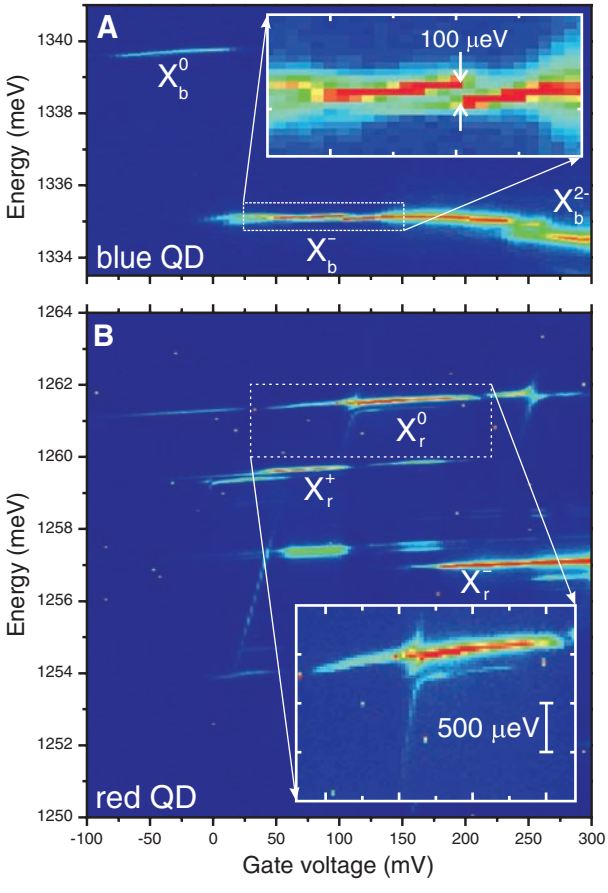

Fig. 2. Low-temperature photoluminescence (in logarithmic color scale) versus gate voltage. (**A**) Recombination involving a hole in the blue dot. PL from the sequence of successively charged exciton complexes leads to the plateaus indicated by the labels. (Inset) The X_b^- transition shifts abruptly by ~100 μeV because of charge sensing of the red QD. (**B**) Recombination involving a hole in the red dot. (Inset) Anticrossing of intradot and interdot recombination for the X_r^0 transition. The normally dark exciton transition is also visible, ~250 μeV below the bright exciton.

tunnel coupling is only substantial near a resonance condition, that is, around specific gate voltages and for specific charge configurations.

This system allows us to realize the conditional scheme depicted in Fig. 1B. In the ground state |1⟩, the blue dot contains a single electron and the red dot is empty (as indicated in the corresponding level diagram). Upon absorption of a photon with the proper energy, a negatively charged exciton |5⟩ is created in the blue dot (X_b^- transition); if a second photon that is resonant with the red X_r^0 transition from state |5⟩ is absorbed, an exciton is created in the red dot as well. Because of electron-hole exchange, the X_r^0 transition is in fact split into two transitions with orthogonal linear polarization, $X_{r,y}^0$ and $X_{r,x}^0$ (*18*, *19*), associated with two slightly nondegenerate states, |6⟩ and |7⟩, respectively. In all of these states (|1⟩, |5⟩, |6⟩, and |7⟩), there is no resonance between the electron levels in the blue and the red dot; thus, the tunnel coupling is not effective (*20*). In contrast, if no photon is absorbed in the blue dot but only in the red dot, then the relevant states |2⟩ and |3⟩ (again split because of electron-hole exchange) are near resonance with the indirect trion state |4⟩, in which both electrons are in the blue dot. Therefore, the tunnel coupling is able to mix states |2⟩, |3⟩, and |4⟩, leading to a shift of their energies. As a result, a photon of the bare energy $X_{r,y}^0$ or $X_{r,x}^0$ can only be absorbed if there is an optical excitation present in the blue dot; this scheme thus describes a conditional operation.

To implement this conditional scheme experimentally, we first characterize a particular stack of two CQDs by performing nonresonant photoluminescence (PL) measurements at 4 K. The substantial blue shift of the bottom QD layer enables us to assign all PL peaks to recombination either involving a hole in the blue QD (Fig. 2A) or involving a hole in the red QD (Fig. 2B). The two QDs behave to a large extent as individual dots because of the relatively thick tunnel barrier between them, so that gate-voltage-dependent PL spectra exhibit the characteristic charging plateaus (*21*) labeled in the figure. For the blue dot, the presence of its red partner only manifests itself in charge sensing (Fig. 2A inset), resulting in a ~100-μeV shift of the negatively charged blue transition (X_b^-) when the red QD charge changes from singly positive (a long-lived metastable state) to neutral (*14*).

The PL spectra for the red QD (Fig. 2B) are considerably more complex. In addition to the standard intradot recombination (between an electron and a hole in the same dot), which exhibits a small Stark shift, we also observe interdot recombination (electron and hole in different dots), which shows a much larger slope because of the relative energy detuning of the dots with gate voltage. For certain gate voltages clear anticrossings appear, indicating mixing between intradot and interdot recombination. The region relevant for this experiment is highlighted in the Fig. 2B inset. In this voltage range,

the lowest energy state of the blue QD has a single excess electron, whereas the red QD ground state is uncharged. The fact that in this region we see evidence of tunnel coupling only for X_r^0 recombination but not for X_b^- tells us unambiguously that the tunnel coupling occurs in the optically excited X_r^0 state but not in the X_b^- state or the ground state. This situation thus corresponds to the mixing between states $|2\rangle$, $|3\rangle$, and $|4\rangle$ that was described in Fig. 1B (*22*).

To probe the conditional behavior of the CQD, we need precise control over the excitons that are created in the system. We used a tunable laser to resonantly excite one of the dots and detected the absorption of the laser by the CQD device with use of the technique of differential transmission (*23*). We can now resolve the 35-μeV electron-hole exchange splitting of the bright neutral exciton in the red QD into the two orthogonal linearly polarized $X^0_{r,y}$ and $X^0_{r,x}$ resonances (compare the rightmost parts of Fig. 3, B and C). For gate voltages around 125 mV (*24*), these two states mix with the indirect trion state, leading to an anticrossing as depicted schematically in Fig. 3D, with a tunnel splitting of 100 μeV. In addition to shifting the transition energies, the mixing also leads to a gradual change in the polarization character of each of the two exchange-split resonances. In contrast to the red dot, the negatively charged exciton transition in the blue dot (X_b^-) shows no indications of tunnel coupling in this voltage range (Fig. 3A), confirming that the tunnel coupling is only present in the excited state of the red dot.

Although single-laser absorption measurements map out the transitions available from the CQD ground state, two simultaneous lasers are required to reveal the effects an optical excitation in one QD has on the states of the partner QD, establishing the conditional interaction of the dots. We measured the absorption of the "red" probe laser (Fig. 3, B and C) but now in the presence of a second "blue" pump laser that is kept on resonance with the X_b^- transition for all gate voltages. In this case, the pump laser can create an optical excitation in the blue dot, giving rise to an extra absorption resonance for each polarization direction of the red laser (blue lines in Fig. 3, E and F). Both of these extra lines follow the linear Stark shift of X_r^0, indicating that they correspond to absorption of a red photon in the absence of tunneling, that is, when the tunnel coupling has been effectively switched off by exciting the blue dot. The appearance of the extra lines (transitions from state $|5\rangle$ to state $|6\rangle$ or $|7\rangle$ in Fig. 1B) thus directly demonstrates the shift of the red QD levels conditional on the state of the blue dot. The original absorption lines of Fig. 3, B and C, are still visible (red lines in Fig. 3, E and F) because the blue dot remains in its ground state at least half of the measurement time, even in the presence of a strong resonant blue laser.

To illustrate the conditional nature of this new resonance more clearly, we present in Fig. 4A the absorption of the red probe laser when the blue pump laser is tuned through the X_b^- resonance of the blue dot (*25*). Both lasers are *y*-polarized, and the gate voltage is fixed at 130 mV, where the effect of the tunnel coupling is substantial. The two tunnel-split resonances already seen in Fig. 3C now show up as two horizontal lines (indicated by the top and bottom horizontal arrows). When the blue laser is resonant with the X_b^- transition (vertical arrow), we again see the strong 30-μeV conditional shift of the red resonance (solid horizontal arrow) and the corresponding strong decrease of the unshifted absorption (*26*).

To verify our interpretation of the experimental data, we modeled the system by using a density-matrix approach, only taking into account the five levels from Fig. 1B that are relevant for *y*-polarized lasers. The energies and lifetimes of these levels were taken from the experiment (*27*), and the absorption was calculated by solving the master equation in Lindblad form in the steady state, as a function of red and blue laser detuning (*28*). The results (Fig. 4B) reproduce all relevant features of the experiment very well. This, in combination with the results of a control experiment in which the roles of the red and blue dot are reversed (fig. S3, B and D), confirms the validity of our model for the conditional interaction.

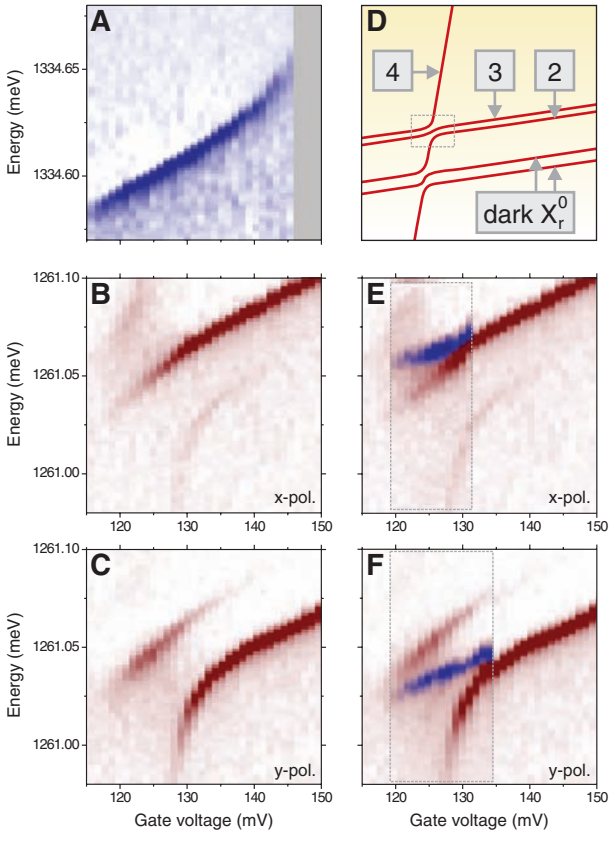

Fig. 3. High-resolution laser absorption mapping out the CQD levels versus gate voltage. (**A**) The X_b^- transition depends linearly on the gate voltage (V_g) below 140 mV, showing no evidence of tunnel coupling. (**B**) Absorption of an *x*-polarized laser reveals the *x*-polarized branch ($X^0_{r,x}$) of the red neutral exciton. (**C**) The *y*-polarized branch ($X^0_{r,y}$), split from $X^0_{r,x}$ because of the electron-hole exchange interaction, is revealed with a *y*-polarized laser. Both resonances anticross with the indirect exciton for $V_g \sim 125$ mV. (**D**) Schematic energy diagram versus gate voltage around the anticrossing. The states are labeled according to the diagram in Fig. 1B. The region relevant for the experiment is indicated in the box. (**E** and **F**) Single-laser absorption as in (B) and (C) in the presence of a second (undetected) blue pump laser, which is kept on resonance with the X_b^- transition for every gate voltage inside the dashed region. This reveals the $X^0_{r,x}$ and $X^0_{r,y}$ when the tunnel coupling has been turned off (blue lines) upon absorption of a blue laser photon, in addition to the original transitions that experience tunnel coupling (red lines). Outside the dashed region, the original data from (B) and (C) are shown.

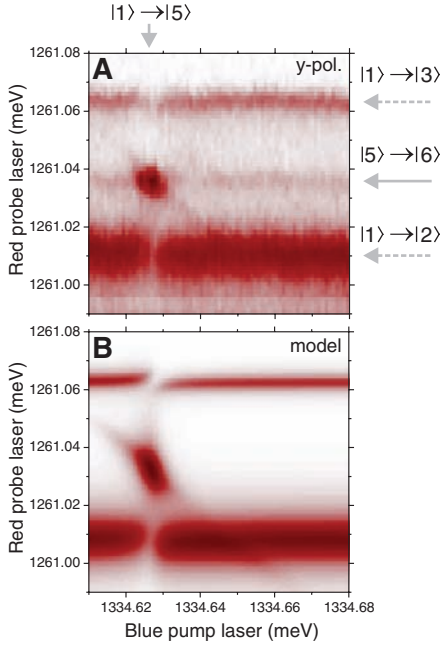

Fig. 4. Two-laser experiment showing conditional interaction in a CQD. Gate voltage is fixed at 130 mV, with *y*-polarized red and blue lasers. (**A**) Absorption of red probe laser in the presence of a strong (undetected) blue pump laser shows a conditional shift of the red QD transition energy when the blue laser is resonant with the X_b^- transition (vertical arrow). (**B**) Calculated absorption for the experiment depicted in (A).

We have demonstrated a method to realize conditional dynamics in a system of two CQDs. The interaction mechanism relies on the tunnel coupling, which can lead to conditional energy shifts that are much larger than those provided by dipole-dipole interactions. More importantly, this tunnel-coupling–mediated interaction can be effectively tuned by changing the energy level detuning via the gate voltage, and it can be optically gated in sub-picosecond time scales by creation of an exciton.

References and Notes

1. P. M. Petroff, A. Lorke, A. Imamoglu, *Phys. Today* **54**, 46 (2001).
2. X. Li *et al.*, *Science* **301**, 809 (2003).
3. M. O. Scully, M. S. Zubairy, *Quantum Optics* (Cambridge Univ. Press, Cambridge, 1997).
4. R. Hanson, L. P. Kouwenhoven, J. R. Petta, S. Tarucha, L. M. K. Vandersypen, *Rev. Mod. Phys.* **79**, 1217 (2007).
5. M. Atatüre *et al.*, *Science* **312**, 551 (2006); published online 5 April 2006 (10.1126/science.1126074).
6. J. Berezovsky *et al.*, *Science* **314**, 1916 (2006); published online 9 November 2006 (10.1126/science.1133862).
7. M. Atatüre, J. Dreiser, A. Badolato, A. Imamoglu, *Nat. Phys.* **3**, 101 (2007).
8. M. Kroner *et al.*, preprint available at http://arxiv.org/abs/0710.4901.
9. M. H. Mikkelsen, J. Berezovsky, N. G. Stoltz, L. A. Coldren, D. D. Awschalom, *Nat. Phys.* **3**, 770 (2007).
10. D. Loss, D. P. DiVincenzo, *Phys. Rev. A* **57**, 120 (1998).
11. J. R. Petta *et al.*, *Science* **309**, 2180 (2005); published online 1 September 2005 (10.1126/science.1116955).
12. H. J. Krenner *et al.*, *Phys. Rev. Lett.* **94**, 057402 (2005).
13. E. A. Stinaff *et al.*, *Science* **311**, 636 (2006); published online 11 January 2006 (10.1126/science.1121189).
14. S. Fält *et al.*, *Phys. Rev. Lett.* **100**, 106401 (2008).
15. T. Calarco, A. Datta, P. Fedichev, E. Pazy, P. Zoller, *Phys. Rev. A* **68**, 012310 (2003).
16. C. Hettich *et al.*, *Science* **298**, 385 (2002); published online 5 September 2002 (10.1126/science.1075606).
17. T. Unold, K. Mueller, C. Lienau, T. Elsaesser, A. D. Wieck, *Phys. Rev. Lett.* **94**, 137404 (2005).
18. M. Bayer *et al.*, *Phys. Rev. B* **65**, 195315 (2002).
19. D. Gammon, E. S. Snow, B. V. Shanabrook, D. S. Katzer, D. Park, *Phys. Rev. Lett.* **76**, 3005 (1996).
20. In principle, states $|1\rangle$ or $|5\rangle$ or $|6\rangle$ and $|7\rangle$ could be split because of electron tunneling, but each of these resonances will only occur at substantially different gate voltages because of the fact that the tunneling strength is much smaller than the relevant Coulomb interaction energies.
21. R. J. Warburton *et al.*, *Nature* **405**, 926 (2000).
22. In the inset, the mixing of the bright X_Y^0 with the indirect exciton is hardly resolved. Clearly visible is the anticrossing of the indirect exciton with the dark X_Y^0, which becomes bright because of the mixing (*14*).
23. B. Alén, F. Bickel, K. Karrai, R. J. Warburton, P. M. Petroff, *Appl. Phys. Lett.* **83**, 2235 (2003).
24. The gate voltage scale for the absorption measurements is slightly different from that of PL because of technical reasons (*28*).
25. To illustrate the observed effect clearly, the intensity of the probe laser is chosen such that it saturates the corresponding ground state transition, whereas the pump laser is set to five times the saturation intensity.
26. In addition to the strong shifted red absorption that occurs for a resonant blue laser (around 1334.63 meV), we also see a weak red absorption around 1261.04 meV even when the blue laser is not resonant. This effect, which is not present when the blue laser is turned off, indicates that even a nonresonant blue laser has a small probability to lift the tunneling resonance between states $|2\rangle$, $|3\rangle$, and $|4\rangle$. This is most likely due to the creation of charges in nearby impurity sites, which can shift the effective gate voltage felt by the CQD. Also, a faint diagonal absorption line is visible around the shifted resonance, which is due to two-photon resonance between states $|1\rangle$ and $|6\rangle$.
27. We have assumed that all excited states are lifetime-broadened.
28. Materials and methods are available on *Science* Online.

29. This work is supported by National Centre of Competence in Research Quantum Photonics (NCCR QP), research instrument of the Swiss National Science Foundation (SNSF), and European Union Research Training Network Engineering, Manipulation, and Characterization of Quantum States of Matter and Light (EMALI). The authors thank K. Weiss for experimental assistance.

Supporting Online Material

www.sciencemag.org/cgi/content/full/320/5877/772/DC1
Materials and Methods
Figs. S1 to S4
References

18 January 2008; accepted 1 April 2008
10.1126/science.1155374

Subnanometer Motion of Cargoes Driven by Thermal Gradients Along Carbon Nanotubes

Amelia Barreiro,[1] Riccardo Rurali,[2] Eduardo R. Hernández,[3]* Joel Moser,[1] Thomas Pichler,[4] László Forró,[5] Adrian Bachtold[1]*

An important issue in nanoelectromechanical systems is developing small electrically driven motors. We report on an artificial nanofabricated motor in which one short carbon nanotube moves relative to another coaxial nanotube. A cargo is attached to an ablated outer wall of a multiwalled carbon nanotube that can rotate and/or translate along the inner nanotube. The motion is actuated by imposing a thermal gradient along the nanotube, which allows for subnanometer displacements, as opposed to an electromigration or random walk effect.

There is a growing effort in the scientific community to design and fabricate ever more versatile nanoelectromechanical systems (NEMS) (*1*). Because carbon nanotubes are very small, mechanically robust, and chemically inert, they have attracted considerable interest as NEMS components. In addition, their one-dimensional tubular shape offers a natural track for motion. This tubular shape restricts the motion (typically translation or rotation) to only a few degrees of freedom, much as bearings do in everyday machines. The tubular track has been the key component for the fabrication of nanotube-based switches (*2*), rotors (*3*, *4*), and mass conveyors (*5*–*7*).

A second generation of nanotube-based motors has been envisaged that takes advantage of the atomic corrugation for a new class of tracks (*8*, *9*). Because the atoms in a nanotube can be arranged in many different configurations, as defined by its chirality, such motors are expected to be quite versatile. For example, a gold nanoparticle confined inside a nanotube is expected to move along a helical orbit around the nanotube axis; this orbit can take different angles and periodicities, which are controlled by the nanotube chirality (*10*, *11*).

The motion of two coaxial nanotubes relative to one another offers additional possibilities, because it combines a pair of chiralities. The track is given by the mutual atomic interaction between the nanotubes. In some cases, the track follows energy minima that can consist of helical orbits ranging from pure rotation to pure translation. In other cases, it contains local minima and maxima, which can be arranged, for example, as a twisted chessboard-like pattern (see some examples in Fig. 1, D to F) (*8*). This flexibility of the energy surface for motion is expected to provide the framework to explore various motion-related phenomena at the nanoscale, such as the ratchet effect (*12*, *13*), vanishingly small friction (*14*), friction resonances (*15*, *16*), and thermal gradient–induced motion (*10*, *11*). However, nanotube motors controlled by the atomic corrugation remain to be experimentally demonstrated.

We report two advances on a nanotube-based motor designed so that motion occurs between two coaxial nanotubes. First, the atomic interaction between the nanotubes is shown to generate distinct kinds of motion for different devices: namely, rotation and/or translation along the nanotube axis. Second, we show that the motion is driven by a thermal gradient. More specifically, the thermal gradient generates a phononic current in one nanotube that hits and drags the second tube. Both findings hold promise for practical use in future NEMS.

[1]Centre d'Investigacions en Nanociencia i Nanotecnologia (Consejo Superior de Investigaciones Científicas–Institut Català de Nanotecnologia) and Centro Nacional de Microelectrónica, Campus de la Universitat Autònoma de Barcelona (UAB), E-08193 Bellaterra, Spain. [2]Departament d'Enginyeria Electrònica, UAB, E-08193 Bellaterra, Spain. [3]Institut de Ciència de Materials de Barcelona, Campus UAB, E-08193 Bellaterra, Spain. [4]Faculty of Physics, University of Vienna, Strudlhofgasse 4, 01090 Wien, Austria. [5]Ecole Polytechnique Fédérale de Lausanne, CH-1015 Lausanne, Switzerland.

*To whom correspondence should be addressed. E-mail: adrian.bachtold@cnm.es (A.B.); ehe@icmab.es (E.R.H.)